Geosci. Model Dev., 11, 1989–2007, 2018
https://doi.org/10.5194/gmd-11-1989-2018

Geoscientific Model Development
Open Access
EGU

Improved regional-scale groundwater representation by the coupling of the mesoscale Hydrologic Model (mHM v5.7) to the groundwater model OpenGeoSys (OGS)

Miao Jing[1], Falk Heße[1], Rohini Kumar[1], Wenqing Wang[2], Thomas Fischer[2], Marc Walther[2,3], Matthias Zink[1], Alraune Zech[1], Luis Samaniego[1], Olaf Kolditz[2,4], and Sabine Attinger[1,5]

[1]Department of Computational Hydrosystems, UFZ – Helmholtz Centre for Environmental Research, Permoserstr. 15, 04318 Leipzig, Germany
[2]Department of Environmental Informatics, UFZ – Helmholtz Centre for Environmental Research, Permoserstr. 15, 04318 Leipzig, Germany
[3]Institute of Groundwater Management, Technische Universität Dresden, Bergstr. 66, 01069 Dresden, Germany
[4]Applied Environmental Systems Analysis, Technische Universität Dresden, Dresden, Germany
[5]Institute of Earth and Environmental Sciences, University of Potsdam, Karl-Liebknecht-Str. 24–25, 14476 Potsdam, Germany

Correspondence: Miao Jing (miao.jing@ufz.de)

Received: 17 September 2017 – Discussion started: 22 September 2017
Revised: 19 April 2018 – Accepted: 10 May 2018 – Published: 1 June 2018

Abstract. Most large-scale hydrologic models fall short in reproducing groundwater head dynamics and simulating transport process due to their oversimplified representation of groundwater flow. In this study, we aim to extend the applicability of the mesoscale Hydrologic Model (mHM v5.7) to subsurface hydrology by coupling it with the porous media simulator OpenGeoSys (OGS). The two models are one-way coupled through model interfaces GIS2FEM and RIV2FEM, by which the grid-based fluxes of groundwater recharge and the river–groundwater exchange generated by mHM are converted to fixed-flux boundary conditions of the groundwater model OGS. Specifically, the grid-based vertical reservoirs in mHM are completely preserved for the estimation of land-surface fluxes, while OGS acts as a plug-in to the original mHM modeling framework for groundwater flow and transport modeling. The applicability of the coupled model (mHM–OGS v1.0) is evaluated by a case study in the central European mesoscale river basin – Nägelstedt. Different time steps, i.e., daily in mHM and monthly in OGS, are used to account for fast surface flow and slow groundwater flow. Model calibration is conducted following a two-step procedure using discharge for mHM and long-term mean of groundwater head measurements for OGS. Based on the model summary statistics, namely the Nash–Sutcliffe model efficiency (NSE), the mean absolute error (MAE), and the interquartile range error (QRE), the coupled model is able to satisfactorily represent the dynamics of discharge and groundwater heads at several locations across the study basin. Our exemplary calculations show that the one-way coupled model can take advantage of the spatially explicit modeling capabilities of surface and groundwater hydrologic models and provide an adequate representation of the spatiotemporal behaviors of groundwater storage and heads, thus making it a valuable tool for addressing water resources and management problems.

1 Introduction

Large-scale hydrologic models had been primarily developed to predict river discharge. To that end, these models typically use simplified representation of underlying hydrological processes, usually bucket-type expressions to describe water storage and flow inside the catchment (Refsgaard and Storm, 1995; Wood et al., 1997; Koren et al., 2004; Samaniego et al., 2010; Niu et al., 2011). Water is transmitted among different vertical and horizontal buckets by means of an infiltration–runoff partitioning algorithm, which can be normally ex-

pressed as a function of the water storage (Hrachowitz and Clark, 2017). Model parameters in these types of models are usually obtained via calibration to match the observed dynamics of streamflow time series. As a result, these types of conceptual models are generally good at predicting streamflow dynamics. However, all (bucket-type) hydrologic models simplify water flow processes by ignoring lateral flow, especially at a large scale. Thus, such models inevitably fall short of characterizing subsurface groundwater dynamics, where such lateral flows are dominant. In addition, estimates of groundwater storage and heads are particularly error prone due to the low sensitivity of groundwater (storage) to river flows.

The groundwater representation in these conceptual (bucket-type) hydrologic models is consequently not adequate in several aspects. First,these models aggregate the heterogeneity of typically stratified groundwater aquifers, and fall short in adequately representing groundwater heads and low-flow conditions (Ameli et al., 2016; Hale and McDonnell, 2016). Second, these models often do not properly capture the dynamics of solute transport and retention at the catchment scale. For example, Van Meter et al. (2017) found that current nitrogen fluxes in rivers can be dominated by groundwater legacies. An oversimplified groundwater representation is inadequate for understanding travel time distributions (TTDs) at a catchment scale and is therefore not capable of describing such legacy behavior (Botter et al., 2010; Benettin et al., 2015, 2017). Finally, a more accurate groundwater representation including lateral subsurface flow is needed to predict the response of groundwater to climate change (Scibek and Allen, 2006; Green et al., 2011; Ferguson et al., 2016).

Parallel to such conceptual surface hydrologic models, three-dimensional (partial differential equation, PDE) subsurface models, which allow for both steady-state and transient groundwater flow, have been developed, accounting for the representation of subsurface heterogeneity and a varying degree of sources and sinks. Such models are good at tackling the aforementioned problems encountered in application of conceptual models. At this end, a variety of numerical codes/models are available such as InHM (VanderKwaak and Loague, 2001; Smerdon et al., 2007), ParFlow (Maxwell and Miller, 2005; Maxwell et al., 2015), OpenGeoSys (Delfs et al., 2012; Kolditz et al., 2012), tRIBS (Ivano et al., 2004), CATHY (Camporese et al., 2010), HydroGeoSphere (Therrien et al., 2010; Hwang et al., 2014), MODHMS (Panday and Huyakorn, 2004; Phi et al., 2013), GEOtop (Rigon et al., 2006), IRENE (Spanoudaki et al., 2009), CAST3M (Weill et al., 2009), PIHM (Kumar et al., 2009; Qu and Duffy, 2007), and PAWS (Shen and Phanikumar, 2010). PDE-based hydrologic models usually represent subsurface flow by accounting for both saturated and unsaturated groundwater flows. The flow fields can be directly computed on the basis of spatial gradients of the modeled primary variable, e.g., the hydraulic head. The PDE-based models are flexible in coping with subsurface heterogeneity by means of proper characterization of the aquifer system (e.g., stratification or geostatistical approach), and thus are able to reduce aggregation errors caused by geological heterogeneity (de Marsily et al., 2005; Cirpka and Attinger, 2003; Zech et al., 2015). Furthermore, these models can explicitly compute flow path lines and provide direct estimates of travel times of water and solute particles. These properties of PDE-based models provide a significant advantage over (bucket-type) conceptual models, especially in complex real-world applications (Park et al., 2008; Engdahl and Maxwell, 2015; Danesh-Yazdi et al., 2018).

However, despite these advantages in modeling the deeper subsurface flows, PDE-based models are not without problems, in particular in capturing the near-surface flow dynamics, i.e., in shallow portions of the subsurface. For example, the PDE-based models often encounter problems in the unsaturated zone for simulating the quick flow components, which are mainly dependent on subgrid heterogeneities of topographic variation as well as soil and land-cover characteristics (Paniconi and Putti, 2015). Using a complex PDE-based surface hydrologic model to simulate near-surface processes is possible in general, but it does require a model implementation at a fine spatial resolution to resolve the subgrid features (e.g., root-water uptake) and include a tremendous number of uncertain model parameters. Furthermore, these models have dramatically increased numerical complexity and computation time, and thus calibrating these models is a cumbersome task, and doing this in a stochastic framework is computationally not feasible.

To summarize these points, bucket-type hydrologic models, such as mHM (Samaniego et al., 2010; Kumar et al., 2013b), VIC (Liang et al., 1994), and HBV (Lindström et al., 1997), are good at predicting water fluxes, such as discharge, but are highly conceptual and their model results are difficult to interpret with respect to certain processes (e.g., groundwater flows). The outputs of PDE-based hydrologic models, such as ParFlow, CATHY, and HydroGeoSphere, are highly interpretable but show consistently worse performance than bucket-type models when predicting discharge dynamics (Gulden et al., 2007; Paniconi and Putti, 2015). The differing capabilities of these two types of models are the result of the different challenges that are posed by the various compartments of the terrestrial water cycle. One of the main challenges in modeling surface and near-surface storage is process uncertainty. The process uncertainty is caused by the strong nonlinearities of hydrological processes and the fine-scale variability in land-surface features. Thus it can hardly be solved by PDE-based models, but it can be well handled by bucket-type models through the parameterization process.

In the deeper subsurface storage, the temporal and spatial scale of groundwater process is significantly larger than the shallow storage, and the flow is governed by linear PDE (Darcy's law), thus making the PDE-based model standard at a large scale (Dagan, 2012). Meanwhile, the data uncertainty becomes more significant in the deep subsurface storage in

comparison to shallow storage due to the spatially sparse hydrogeological data. Moreover, a recent study reveals the strong spatial and temporal heterogeneity of processes and properties at the surface water–groundwater (SW–GW) interface, and underlines the importance of quantifying variability across several scales at the SW–GW interface and its significance to water resources management (McLachlan et al., 2017). It therefore stands to reason that the use of a hybrid of both these model frameworks is a good choice for a joint representation of surface and subsurface water storages and fluxes. Therefore, the coupling between the bucket-type land-surface model and the subsurface saturated–unsaturated groundwater model is highly relevant. Several well-tested coupled models have been developed in recent years, including ParFlow-CLM (Maxwell and Miller, 2005; Maxwell et al., 2015; Kurtz et al., 2016), GSFLOW (Markstrom et al., 2008; Hunt et al., 2013), PCR-GLOBWB-MOD (Sutanudjaja et al., 2011, 2014), and CP(v1.0) (Bisht et al., 2017).

In this study, we present a coupling between the conceptual mesoscale Hydrologic Model (mHM v5.7) and the PDE-based model OpenGeoSys (OGS) (Kolditz et al., 2012, 2016). The overall aim is to provide a proper representation of groundwater flows and storages and enabling the coupled model to provide reliable estimates of groundwater heads. mHM has demonstrated its preeminence in coping with near-surface process uncertainty while providing reliable representation of observed discharge behavior across a range of scales and locations (Samaniego et al., 2010; Kumar et al., 2013b; Huang et al., 2017). Conversely, OGS has demonstrated its capability of dealing with data uncertainty in aquifers (Sun et al., 2011; Walther et al., 2012; Selle et al., 2013). The general idea behind the coupling is to use the hydrological simulation with mHM, including the simplified linear groundwater storage, extract fluxes into and out of groundwater from mHM, and use this as the Neumann boundary condition for the PDE-based groundwater model OGS. By doing so, we augment the predictive power of mHM to also predict hydraulic heads in groundwater. The one-way coupling approach considered here has a number of advantages. First, the one-way coupling can be regarded as a conservative approach, such that the parametrization process, which is one of the most significant features of mHM, remains fully intact. In particular, this means that the whole body of confidence in the predictive power of mHM, which has been built up over the years, can be fully relied on. Second, using such a one-way coupling will allow users of mHM to simply extend currently established catchment models and enhance their abilities in the aforementioned way. Using a more sophisticated two-way coupling would entail users having to rebuild their models almost entirely. Third, a one-way coupling allows for ready future expansion of the functionality of the coupled model, e.g., legacy of solutes in groundwater, should the need arise. Finally, one-way coupling takes less computational effort and achieves better numerical stability than two-way coupling.

By coupling two well-tested model codes, we want to answer the following scientific questions: (1) can spatially distributed groundwater heads and their dynamics be reasonably captured by expanding the capabilities of a surface hydrologic model, such as mHM at the regional scale, while conserving its excellence in predicting discharge? (2) Can spatially resolved groundwater recharge estimates, provided by mHM, improve the prediction of head measurements of groundwater models such as OGS? To answer these questions, we applied the coupled model mHM–OGS v1.0 in a central German mesoscale catchment (850 km^2), and evaluated the model skills using measurements of streamflow and groundwater heads from several wells located in the study area. The coupled (surface) hydrologic and groundwater model (mHM–OGS v1.0) presented in this paper is our first attempt toward the development of a large-scale coupled modeling system with the aim to analyze the spatiotemporal variability in groundwater flow dynamics at a regional scale.

To answer these questions, the paper is structured as follows. In the next section, we describe the model concept, model structure, and the coupling scheme. In Sect. 3.1, the study area and model setup used for illustration in this study are comprehensively described. In Sect. 4, we present the simulation results of mHM–OGS v1.0 in a catchment in the application. In Sect. 5, we discuss the model results as well as advantages and limitations of the current modeling approach.

2 Model description

2.1 Mesoscale Hydrologic Model (mHM)

The mesoscale Hydrologic Model (mHM, www.ufz.de/mhm) is a spatially explicit distributed hydrologic model that uses grid cells as a primary modeling unit, and accounts for the following processes: canopy interception, snow accumulation and melting, soil moisture dynamics, infiltration and surface runoff, evapotranspiration, subsurface storage and discharge generation, deep percolation, baseflow, discharge attenuation, and flood routing (Fig. 1). The runoff generation applies a robust scheme, which routes runoff in upstream cells along river networks using the Muskingum–Cunge algorithm. The model is driven by daily meteorological forcings (e.g., precipitation, temperature), and utilizes observable physical properties or signals of the basin (e.g., soil textural, vegetation, and geological properties) to infer the spatial variability in the required parameters. mHM is an open-source project written in Fortran 2008. Parallel versions of mHM using OpenMP concepts are available.

A unique feature of mHM is the application of multi-scale parameter regionalization (MPR). The MPR method accounts for subgrid variability in physical characteristics of the catchment such as topography, soil, and vegetation. The MPR methodology facilitates the flexibility of the model for hydrological simulations at various spatial

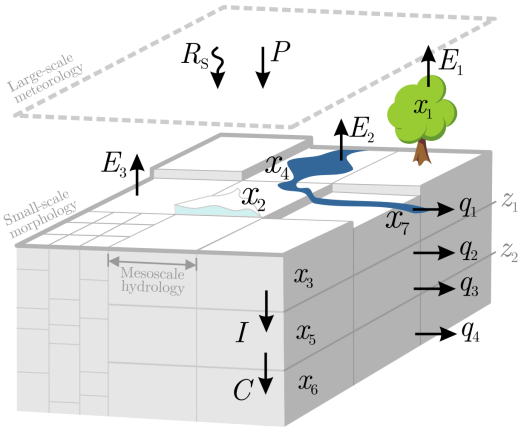

Figure 1. The concept of the mesoscale hydrologic model, mHM.

scales (Samaniego et al., 2010, 2017; Kumar et al., 2013a, b; Rakovec et al., 2016a, b). mHM differentiates three levels to better represent the spatial variability in state and input variables. The effective parameters at different spatial scales are dynamically linked by a physically based upscaling scheme. A detailed description of MPR, as well as the formulations governing hydrological processes, is given by Samaniego et al. (2010) and Kumar et al. (2013b).

Below, we list the equations that describe near-surface processes in the deep soil and groundwater layers. The comprehensive system of equations of mHM can be found in Samaniego et al. (2010). Here, we only listed the equations needed for the coupling. In the subsurface reservoir, which is the second vertical layer (x_5 in Fig. 1), interflow is partitioned into fast interflow (q_2) and slow interflow (q_3):

$$q_2(t) = \max\{I(t) + x_5(t-1) - \beta_1(z_2 - z_1),\ 0\}\beta_2, \quad (1)$$

$$q_3(t) = \beta_3(x_5(t-1))^{\beta_4}, \quad (2)$$

where $q_2(t)$ is fast interflow at time t [$\mathrm{L\,T^{-1}}$], I is the infiltration capacity [L], x_5 is the water depth of water storage in the deep soil reservoir [L], β_1 is the maximum holding capacity of the deep soil reservoir [–], z_i is depth of the subsurface layer i [L], β_2 is the fast-recession constant [$\mathrm{T^{-1}}$], $q_3(t)$ is slow interflow at time t [$\mathrm{L\,T^{-1}}$], β_3 is the slow-recession constant, and β_4 is the exponent that quantifies the degree of nonlinearity of the cell response.

The groundwater recharge is equivalent to the percolation to the groundwater reservoir (the third vertical layer; see x_6 in Fig. 1). The groundwater recharge $C(t)$ can be expressed by

$$C(t) = \beta_5 x_5(t-1), \quad (3)$$

where $C(t)$ is the groundwater recharge in cell i [$\mathrm{L\,T^{-1}}$], and β_5 is the effective percolation rate coefficient [$\mathrm{T^{-1}}$].

In the groundwater reservoir, baseflow is generated following a linear relationship between storage and runoff:

$$q_4(t) = \beta_6 x_6(t-1), \quad (4)$$

where $q_4(t)$ is the baseflow [$\mathrm{L\,T^{-1}}$], β_6 is the baseflow recession rate coefficient [$\mathrm{T^{-1}}$], and x_6 is the depth of the groundwater reservoir [L].

The runoff from upstream grid cells and the internal runoff in cell i are routed into streams using the Muskingum algorithm:

$$Q_i^1(t) = Q_i^1(t-1) + c_1(Q_i^0(t-1) - Q_i^1(t-1)) + c_2(Q_i^0(t) - Q_i^0(t-1)), \quad (5)$$

with

$$Q_i^0(t) = Q_{i'}(t) + Q_{i'}^1(t), \quad (6)$$

$$c_1 = \frac{\Delta t}{\kappa(1-\xi) + \frac{\Delta t}{2}}, \quad (7)$$

$$c_2 = \frac{\frac{\Delta t}{2} - \kappa\xi}{\kappa(1-\xi) + \frac{\Delta t}{2}}, \quad (8)$$

where Q_i^0 and Q_i^1 denote the runoff entering and leaving the river reach located in cell i [$\mathrm{L\,T^{-1}}$], respectively, $Q_{i'}$ is the contribution from the upstream cell i' [$\mathrm{L\,T^{-1}}$], κ is the Muskingum travel time parameter [T], ξ is the Muskingum attenuation parameter [–], Δt is the time step size [T], and t is the time index for each Δt interval.

2.2 OpenGeoSys (OGS)

OpenGeoSys (OGS) is an open-source project with the aim of developing robust numerical methods for the simulation of thermo–hydro–mechanical–chemical (THMC) processes in porous and fractured media. OGS is written in C++ with a focus on the finite element analysis of coupled multifield problems. Parallel versions of OGS based on both MPI and OpenMP concepts are available (Wang et al., 2009, 2017; Kolditz et al., 2012). To date, two OGS versions are available: OGS5 (https://github.com/ufz/ogs5, last access: 30 May 2018) and OGS6 (https://github.com/ufz/ogs, last access: 30 May 2018). In this study, the term "OpenGeoSys (OGS)" represents OGS5 if not stated otherwise.

OGS has been successfully applied in different fields, such as water resources management, hydrology, geothermal energy, energy storage, CO_2 storage, and waste disposal (Kolditz et al., 2012; Shao et al., 2013; Gräbe et al., 2013; Wang et al., 2017). In the field of hydrology–hydrogeology, OGS has been applied to regional groundwater flow and transport (Sun et al., 2011; Selle et al., 2013), contaminant hydrology (Beyer et al., 2006; Walther et al., 2014), reactive transport (Shao et al., 2009; He et al., 2015), and seawater intrusion (Walther et al., 2012), among others.

Saturated groundwater flow follows the continuity equation and Darcy's law:

$$S\frac{\partial \psi_p}{\partial t} = -\nabla \cdot \boldsymbol{q} + q_s, \quad (9)$$

$$\boldsymbol{q} = -K_s \nabla(\psi_p + z), \quad (10)$$

where S is the specific storage coefficient in confined aquifers, and the specific yield in unconfined aquifers [L^{-1}], ψ_p is the pressure head in the porous medium [L], t is time [T], $\boldsymbol{q}$ is the specific discharge or Darcy velocity [$L\,T^{-1}$], q_s is the general source or sink term [T^{-1}], K_s is the saturated hydraulic conductivity tensor [$L\,T^{-1}$], and z is the vertical coordinate (positive upward) [L].

The stream network is normally represented by a set of polylines in the geometry file of OGS. In the case of a 3-D model, a common way to set up the polyline system is to utilize the mapping tool embedded in OGS source codes, by which the shape file obtained from GIS software representing streams can be easily mapped onto the upper surface of OGS mesh and converted into a set of polylines. Each reach of the stream network can be represented by one polyline or several continuous polylines, depending on the demand of the user. Each polyline consists of a set of continuous mesh nodes, to which Dirichlet, Neumann, or Robin boundary conditions can be applied.

2.3 Coupling mechanism

The coupled model mHM–OGS v1.0 is developed to simulate SW–GW flow in one or more catchments by simultaneously calculating flow across the land surface and within the groundwater. mHM–OGS v1.0 simulates flow within three hydrological regions. The first region is limited by the upper boundary of the plant canopy and the lower boundary of the soil zone bottom. The second region includes open-channel water, such as streams. The third region is the water-saturated aquifer. mHM is used to simulate the processes in the first and second regions, while OGS is used to simulate the groundwater flow for prescribed fluxes at all boundaries in the third region.

The coupling initiative aims to add additional predictive capability of groundwater heads, which is achieved by OGS, to the existing capability of predicting discharges that is achieved by mHM. mHM is used to estimate a water budget stepwise and component-wise through model calibration against discharge. In contrast, OGS serves as a post-processor to obtain groundwater heads by using mHM-simulated recharge and baseflow as driving forces. Two model interfaces, namely GIS2FEM and RIV2FEM, have been developed to link the two models by transferring recharge and baseflow from mHM to Neumann boundary conditions in OGS.

The two models are executed separately and sequentially, typically with different temporal (e.g., daily in mHM and weekly or monthly in OGS) and spatial resolutions (e.g., rectangular, structured grids with coarse resolution in mHM and smaller, potentially unstructured grids with fine resolution in OGS). The original vertically layered reservoirs in mHM, namely the soil-zone reservoir and the subsurface reservoir, are preserved, implying that all well-tested features of mHM (e.g., MPR, infiltration–runoff partitioning) are retained in the coupled model.

To illustrate the coupling mechanism in detail, we itemized the coupling workflow below.

1. mHM is run independently of OGS to calculate land surface fluxes including exchange fluxes of the groundwater storage.
   Using gridded meteorological forcings (precipitation, temperature, and potential evapotranspiration), the grid-based infiltration rates (e.g., groundwater recharge) and runoff components (e.g., interflow, baseflow) are estimated and saved as mHM output files. The original linear groundwater reservoir (depth x_6 in Fig. 1) is used to estimate baseflow. Moreover, MPR is used in the calibration process such that subgrid variabilities can be validly calculated. The spatially distributed groundwater recharge and total routed baseflow are written into raster files for later use.

2. After the mHM run has finished, the stepwise routed baseflow estimated by mHM is transformed to distributed river discharges along streams and spatially distributed exchange rates between streams and groundwater needed in OGS.
   Most PDE-based models characterize river–groundwater interaction based on either first-order flow exchange or boundary condition switching (Paniconi and Putti, 2015). However, these approaches inevitably introduce extra parameters describing geometric, topographic, and hydraulic properties of the stream channel (e.g., river bed conductance, river bed and drain elevations, channel width). Unfortunately, these parameters are essentially unknown at a large scale due to the lack of data and the subgrid-scale variability in these parameters. Due to these limitations, we use an alternative approach, which is based on the routed baseflow estimated by mHM.
   mHM and OGS conceptualize streams differently: streams in mHM are implicitly defined based on pre-processing of digital elevation model (DEM) data and a routing scheme, while OGS uses an explicit predefined river geometry. In OGS, each reach of the stream network is defined by a polyline in the OGS geometry file. To coordinate the two different approaches, we developed a model interface, RIV2FEM, to convert the routed baseflow estimated by mHM to Neumann boundary conditions assigned at stream nodes of the OGS mesh (Fig. 2d). Via RIV2FEM, the routed baseflow estimated by mHM is transferred to the uniformly disaggregated groundwater discharges by distributing it

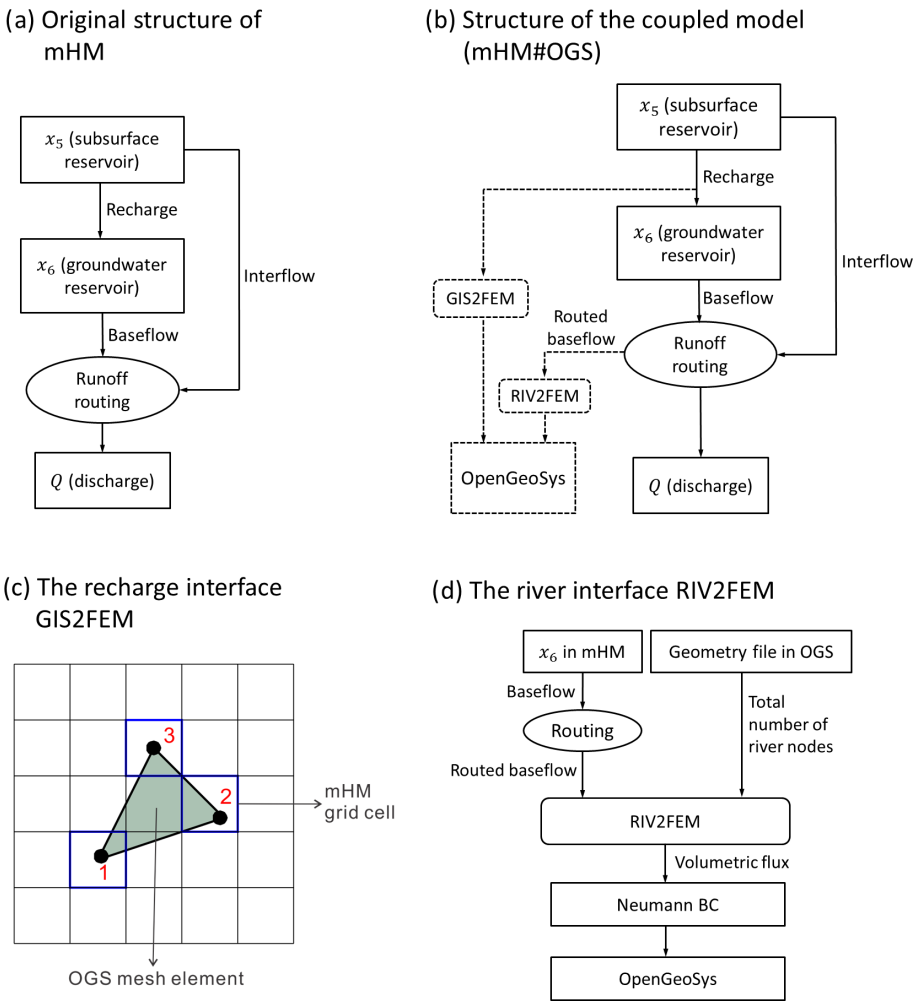

Figure 2. Schematic of the coupled model mHM–OGS v1.0. **(a)** Original structure of the vertically layered reservoir of mHM. **(b)** Structure of the coupled model (mHM–OGS v1.0). **(c)** Illustration of data interpolation and transformation through the coupling interface GIS2FEM. **(d)** Scheme of the river interface RIV2FEM. For the sake of simplicity, the figure only displays mHM layers relevant to this study and neglects the other mHM layers (i.e., $x_1 - x_4$). In **(c)**, the grid-based mHM fluxes (e.g., recharge) are linearly interpolated to the top surface of the OGS mesh and further transferred into volumetric values and directly assigned to the surface mesh nodes of the OGS grid.

uniformly along the predefined stream network in OGS (Fig. 2d):

$$\overline{q}_4(t) = \frac{Q_4(t)}{\sum_{i=1}^{N} A_i}, \tag{11}$$

where $\overline{q}_4(t)$ denotes the normalized flux of disaggregated groundwater discharge at time t [$\mathrm{L\,T^{-1}}$], $Q_4(t)$ denotes the routed baseflow at the outlet of catchment at time t [$\mathrm{L^3\,T^{-1}}$], A_i is the nodal area of the ith stream node [$\mathrm{L^2}$], and N is the total number of stream nodes. The uniformly disaggregated groundwater discharges are then assigned to every stream node in OGS to serve as the Neumann boundary condition (Fig. 2d). This approach significantly reduces the number of parameters, avoids the uncertainty caused by the unknown river properties, and is suitable for many real-world applications that suffer from scarce data. Moreover, as recharge and baseflow are directly taken from mHM, the mass conservation criterion is naturally satisfied in this approach.

3. The distributed groundwater recharge generated by mHM is fed to the coupling interface GIS2FEM, and then transferred to the upper surface boundary conditions of the OGS model.
   The coupling interface GIS2FEM is used to interpolate and transfer mHM grid-based recharge to OGS nodal recharge values. GIS2FEM interpolates the flux value to the top surface elements of the OGS mesh. The detailed workflow is

   – GIS2FEM reads the raster file generated by mHM and the mesh file of OGS.

- In the case of a 3-D mesh, GIS2FEM extracts the upper surface of the OGS mesh. For each of the nodes on this surface, GIS2FEM searches for the mHM grid cell that the node is located in, and assigns the recharge value of this grid cell to the corresponding node (marked as C^{m}).

- After all top surface elements have been processed, GIS2FEM undertakes the face integration calculation, by which the specific recharge C^{m} [$\mathrm{L\,T^{-1}}$] calculated by mHM is converted into volumetric recharge C^{in} [$\mathrm{L^3\,T^{-1}}$] and assigned to the corresponding OGS mesh nodes (Fig. 2c). Specifically, the specific recharge C in a certain element is calculated as

$$C(x) = \sum_{i=1}^{N} W_i(x) C_i^{\mathrm{m}}, \tag{12}$$

where x is the spatial coordinate on the surface, N is the total number of nodes in a surface element, W_i is the weighting function of ith node of the OGS surface element, and C_i^{m} is the specific recharge at the ith node of the OGS surface element (calculated by mHM) [$\mathrm{L\,T^{-1}}$]. Then the volumetric recharge C_i^{in} at the ith node (here i is the global node index) is calculated by the face integration calculation:

$$C_i^{\mathrm{in}} = -\int_{\partial\Omega} W_i(x) C(x) \mathrm{d}(x), \tag{13}$$

where C_i^{in} is the volumetric recharge of node i [$\mathrm{L^3\,T^{-1}}$], $\partial\Omega$ is the surface boundary of the finite element method (FEM) domain, and W_i is the weighting function of the ith node.

4. After the mHM-generated recharge and baseflow have been transferred into boundary conditions at the upper surface of the OGS mesh, the groundwater model is run to simulate the groundwater flow and transport.
   In this step, additional boundary conditions can be set up in OGS mesh on the basis of expert knowledge. The exclusive use of Neumann boundary conditions is not recommended and may lead to nonuniqueness of solutions. At least one specified head boundary should be set at the perimeter or internal nodes to constrain the model solution. The groundwater model simulates groundwater flow to obtain hydraulic heads in the example application. The groundwater model may also be used to compute travel times and solute transport within the groundwater domain, requiring additional boundary conditions; but this is not described in the present paper.

3 Example application

3.1 Study area and model setup

We use a mesoscale catchment (about 850 $\mathrm{km^2}$) upstream of the Nägelstedt gauge located in central Germany to test our coupled model (Fig. 3). The Nägelstedt catchment comprises the headwaters of the Unstrut River, a tributary of the river Saale. We selected this study area because many of the groundwater monitoring wells in the area are operated by the Thuringian State Office for the Environment and Geology (TLUG) and the Collaborative Research Center AquaDiva (Küsel et al., 2016). The elevation within the catchment ranges between 164 and 516 m, whereby the higher regions are in the west and south and belong to the forested hill chain of the Hainich (Fig. 3). The Nägelstedt catchment is one of the most intensively used agricultural regions in Germany. In terms of drinking water supply, about 70 % of the water requirement is satisfied by groundwater (Wechsung, 2005). About 17 % of the land in this region is forested area, 78 % is covered by crop and grassland, and 4 % is urban and transport area. The mean annual precipitation in this area is about 660 mm.

In this study, mHM runs were executed for a time period of 35 years (from 1 January 1970 to 30 December 2004), with the period 1970–1974 being used for spin-up. OGS was run for the period from 1 January 1975 to 30 December 2005. mHM was run with a daily time step, while OGS was run with a monthly time step. The resolution of mHM grid cells is 500 m × 500 m. OGS uses a structured, hexahedral 3-D mesh, with a spatial resolution of 250 m × 250 m in the horizontal direction and 10 m in the vertical direction over the whole domain. The detailed input data and parameter set to run both models are detailed in the following sections.

3.2 Meteorological and surface properties

We started the modeling by performing the daily simulation of mHM to calculate near-surface hydrological processes. The mHM model is forced by daily meteorological conditions, including distributed precipitation and atmospheric temperature. The spatial patterns of precipitation and atmospheric temperature were based on point measurements of precipitation and atmospheric temperature at weather stations from the German Meteorological Service (DWD). The point data at weather stations were subsequently kriged onto a 4 km precipitation field, and then downscaled to mHM grid cells. Moreover, the potential evapotranspiration (ET) was estimated based on the method from Hargreaves and Samani (1985). Other datasets used in mHM are the DEM data, which are the basis for deriving properties such as slope, river beds, and flow direction; soil and geological maps, derived properties such as sand and clay contents, and bulk density; CORINE land-cover information (in the years 1990, 2000, and 2005); and discharge data at the outlet of the catchment.

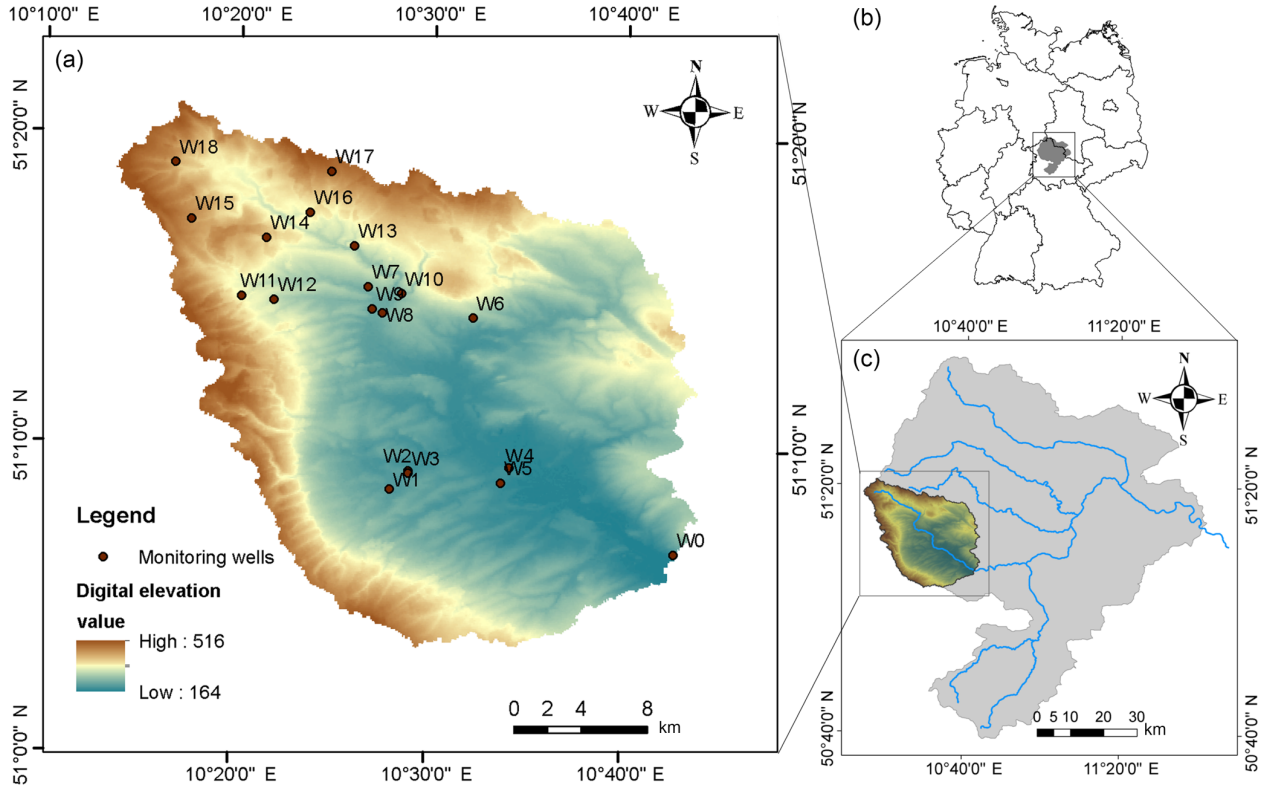

Figure 3. The Nägelstedt catchment used as the test catchment for this study. Panel **(a)** shows elevation and locations of monitoring wells used in this study. Panel **(c)** shows the relative location of the Nägelstedt catchment in the Unstrut basin. Panel **(b)** shows the location of the Unstrut basin in Germany.

3.3 Aquifer properties

We used a stratigraphic model to explicitly represent the heterogeneous distribution of hydraulic properties (hydraulic conductivity, specific yield, and specific storage). The stratigraphic model is based on well log data and geophysical data obtained from the TLUG. We used the workflow developed by Fischer et al. (2015) to convert the data format, by which the complex 3-D geological model was converted into the open-source VTK format file that can be directly read by OGS.

The major stratigraphic units in the study site are the Muschelkalk (Middle Triassic) and the Keuper (Upper Triassic). Younger Tertiary and Quaternary deposits are less important for the large-scale hydrogeology of the basin. The Keuper deposits mainly lie in the center of the Unstrut basin and act as permeable shallow aquifers. In the Nägelstedt catchment, the Keuper deposits are further subdivided into two geological sub-units: Middle Keuper (km) and Lower Keuper (ku) (see Fig. 4). The Muschelkalk is marked by a prevailing marine environment and is subdivided into three sub-units the Upper Muschelkalk (mo), Middle Muschelkalk (mm, dolomites and residues of eroded salt layers), and Lower Muschelkalk (mu, limestones). According to previous geological surveys (Seidel, 2004), the sub-units of the Muschelkalk have varying hydraulic properties depending on their positions and depths. They are further divided into sub-units with higher permeabilities (mo1, mm1, and mu1) and sub-units with lower permeabilities (mo2, mm2 and mu2) (Fig. 4). The mo has been widely considered to be a karstified formation. Recent research by Kohlhepp et al. (2017) has revealed that in the Hainich Critical Zone, the intense karstification and the conduit are limited at the base of the mo formation. Accordingly, we use the equivalent porous medium approach to characterize the mo. The uppermost layer with a depth of 10 m is set as a soil layer (Fig. 4). A high-permeability alluvium layer is set along the mainstream and major tributaries to represent granite and stream deposits (Fig. 4).

3.4 Boundary conditions

Based on the steep topography along the watershed divides, groundwater is assumed to be naturally separated and unable to pass across the boundaries of the watershed. In general, no-flow boundaries are set at the outer perimeters surrounding the basin as well as at the lower aquitard, except for the northwestern and northeastern edges. On the basis of the measurements, a Dirichlet boundary condition is assumed at the northwestern and northeastern edges.

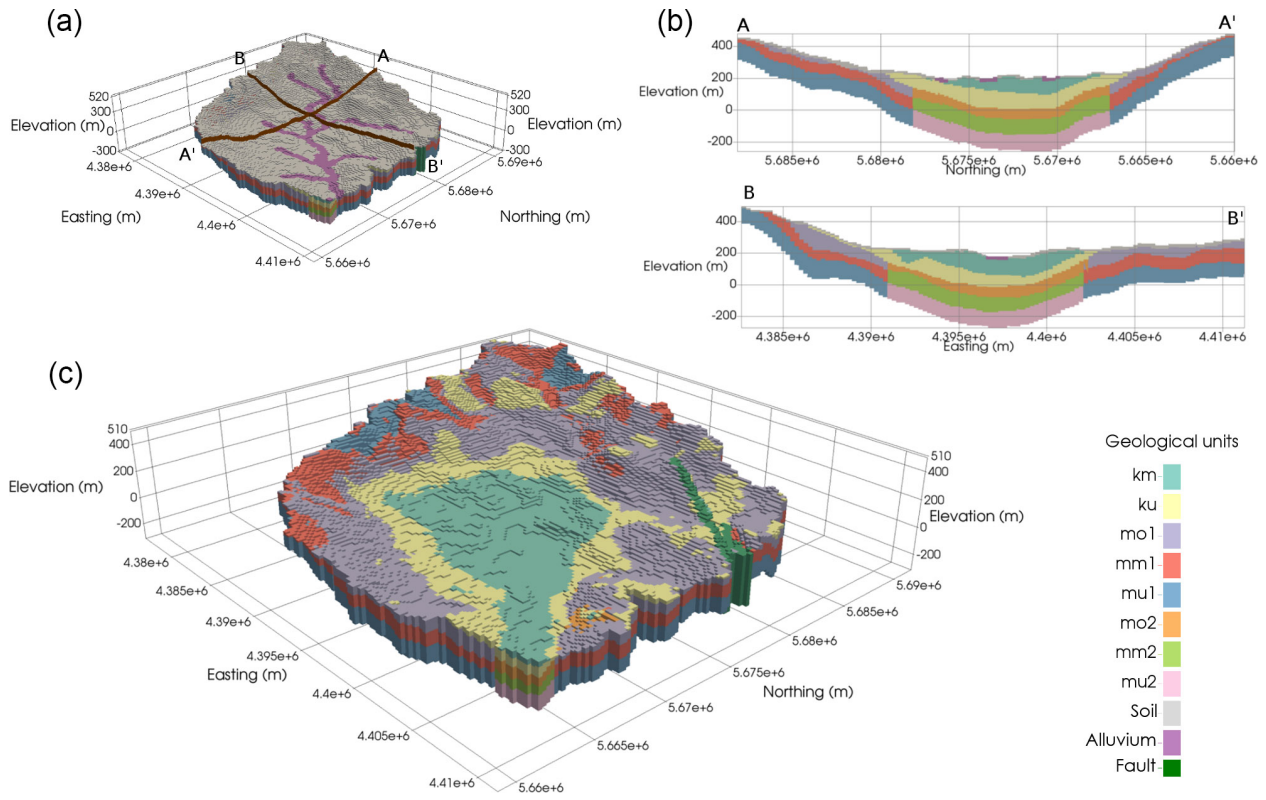

Figure 4. Three-dimensional and cross-sectional views of the hydrogeologic zonation in the Nägelstedt catchment. Panel **(a)** highlights the distribution of alluvium and soil zones. Panel **(b)** shows two vertical geological cross sections. Panel **(c)** shows the detailed zonation of geological sub-units beneath the soil zone and alluvium.

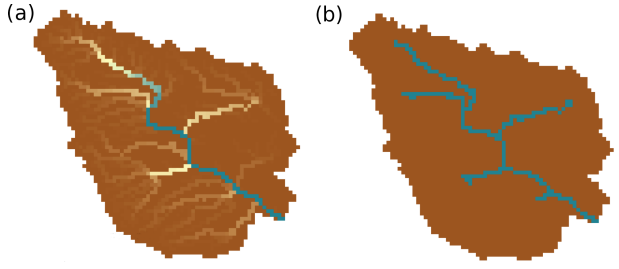

Figure 5. Illustration of the stream network used in this study. **(a)** Original stream network based on the streamflow routing algorithm of mHM; **(b)** processed stream network that was used in this study. The small tributaries where the runoff rates are below the threshold ($0.145\,m^3\,s^{-1}$) as shown in panel **(a)** have been removed to form panel **(b)**.

The stream network was delineated by processing a grid-based runoff raster file generated by mHM. The grid-based runoff was converted to a valid stream network compatible with OGS. The necessity of transferring the mHM runoff raster file to the OGS stream network has been elaborated in Sect. 2.3. Particularly in this case study, we removed the small intermittent tributaries by setting a threshold value of long-term averaged routed runoff. Only streams with a runoff rate higher than the threshold (in this case study, $0.145\,m^3\,s^{-1}$) are delineated as valid streams. In other words, we neglected the intermittent streams to the upper stream reaches (Fig. 5). The preprocessed stream network consists of a main stream and four tributaries (Fig. 5b). The reach of each stream is defined as a polyline in a geometry file. As illustrated in Sect. 2.3, uniformly disaggregated groundwater discharges processed by the interface RIV2FEM were assigned to every OGS mesh node within the stream network.

3.5 Calibration procedure

The calibration of the coupled model follows a two-step procedure. In the first step, mHM was calibrated independently of OGS for the period from 1970 to 2005 by matching the observed runoff at the outlet of the catchment. The first 5 years were used as spin-up period to set up initial conditions in the near-surface soil zone. The calibration quality is quantified by the Nash–Sutcliffe coefficient of efficiency (NSE):

$$\mathrm{NSE} = 1 - \frac{\sum_{i=1}^{n} |(q_\mathrm{m} - q_\mathrm{s})|_i^2}{\sum_{i=1}^{n} |(q_\mathrm{m} - \overline{q}_\mathrm{m})|_i^2}, \tag{14}$$

where q_s is the simulated discharge [$L^3\,T^{-1}$], q_m is the measured discharge [$L^3\,T^{-1}$], and $\overline{q}_\mathrm{m}$ is the mean of measured discharge [$L^3\,T^{-1}$].

In the second step, the steady-state groundwater model in OGS was calibrated to match the long-term mean of observed groundwater levels. The long-term mean of recharge and baseflow estimated by mHM were fed to the steady-state groundwater model as Neumann boundary conditions. The calibration was performed using the software package PEST (Doherty, 1994). The model parameters were adjusted within a fixed interval until the value of objective function, which is the sum of weighted squared residuals of modeled and observed groundwater heads, was minimized. Specifically, the intervals of adjustable parameters were taken from the literature (Wechsung, 2005; Seidel, 2004), and the weights assigned to each observation were set uniformly to 1. The calibration result is assessed using the root-mean-square error (RMSE).

3.6 Model evaluation and sensitivity analysis

We used the time series of groundwater levels in 19 monitoring wells to evaluate the predictive capability of the transient model. In the transient model, hydraulic conductivities are obtained from the calibrated steady-state model. Meanwhile, the initial condition of the groundwater head is directly taken from the result of the steady-state model. The Pearson correlation coefficient R_{cor} and the interquartile range error (QRE) are used as two summary statistics to evaluate the predictive capability. The (relative) QRE is defined by

$$\mathrm{QRE} = \frac{\mathrm{IQ}^{\mathrm{md}}_{7525} - \mathrm{IQ}^{\mathrm{dt}}_{7525}}{\mathrm{IQ}^{\mathrm{dt}}_{7525}}, \tag{15}$$

where $\mathrm{IQ}^{\mathrm{md}}_{7525}$ and $\mathrm{IQ}^{\mathrm{dt}}_{7525}$ are the interquartile ranges of simulations and observations, respectively.

We sought to quantify the sensitivity of groundwater flows to the different spatial pattern of recharge. For this purpose, a uniform recharge scenario was established as the reference scenario. The sensitivity analysis follows a two-step workflow. First, we calibrated the steady-state groundwater models for the two recharge scenarios independently. Second, we conducted transient simulations by assigning the same values of storage parameters, and then observed their corresponding performances in two recharge scenarios. With the exception of recharge scenario and hydraulic-conductivity values, all model parameters (e.g., specific yield and specific storage) and inputs are set to be identical in both scenarios. The mean absolute error (MAE) and the QRE are used as two summary skill scores to assess model performances in the two recharge scenarios.

4 Results

4.1 Calibration

As the first part of calibration, mHM is calibrated against discharge. The calibration results demonstrate the predictive capability of mHM in reproducing the time series of catchment discharge (Fig. 6). The NSE is 0.88. Other fluxes, such as evapotranspiration measured at eddy-covariance stations inside this area, also show quite reasonable correspondence to the modeled estimate (Heße et al., 2017).

In the second step, the steady-state groundwater model is calibrated against the long-term mean of groundwater heads. Table 1 shows the calibrated hydraulic conductivities in each of the geological units. The objective function of calibration, which is the sum of squared, weighted residuals, converged from an initial value of 8625 to 464.74 m^2 after a total of 114 model runs. Broadly speaking, the steady-state model can plausibly reproduce the finite numbers of observed groundwater heads in the catchment. Figure 7 shows the one-to-one plot of simulated and observed groundwater heads (locations of those wells are shown in Fig. 3). In general, the model is capable of reproducing spatially distributed groundwater heads over a wide range, with an overall RMSE of 6.45 m. Most of the discrepancies between individual observations and simulations are within a reasonable range (i.e., less than 6 m). Nevertheless, some monitoring wells show larger discrepancies between observations and simulations (i.e., greater than 6 m), which is due to the unknown local or even subgrid-scale properties. For the sake of simplicity, no further attempt was made to add more model complexity to improve the model fit.

The simulated depth to groundwater over the whole catchment using the calibrated hydraulic-conductivity values is shown in Fig. 7c. Broadly speaking, the calibrated model reasonably reproduces the spatial groundwater table distribution. Groundwater depth varies between greater than 40 m in the higher southwestern and northern mountainous areas and less than 5 m in the central lowlands. The plausibility of steady-state simulation results can be assessed through regionalized observations of groundwater heads (Wechsung, 2005).

4.2 Spatiotemporal patterns of recharge and baseflow

Groundwater recharge has a spatially variable and dynamic behavior depending on the sporadic, irregular, and complex features of precipitation, geological structure, and morphological features. The temporal and spatial variability in groundwater recharge and baseflow is estimated by mHM over a period of 30 years from 1975 to 2005.

Figure 8 shows the spatial variability in groundwater recharge in three months: March (Fig. 8a), May (Fig. 8b), and January (Fig. 8c). The results indicate that the location of the highest recharge rate is in the upstream mountainous areas where the Muschelkalk aquifer crops out, but it varies in different seasons. The maximum value of monthly groundwater recharge varies from 26 mm in March to 51 mm in May and 14 mm January. We also evaluated the plausibility of groundwater recharge simulated by mHM through comparison to other reference datasets. At the large scale, the groundwater

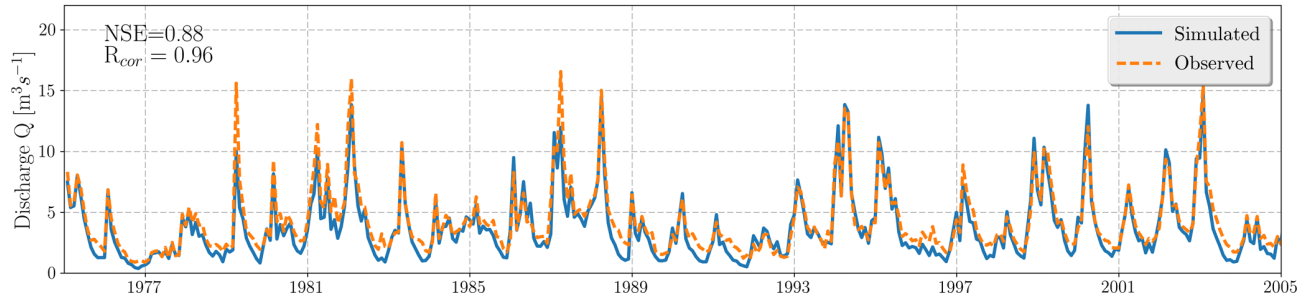

Figure 6. Observed and simulated monthly discharge at the outlet of the Nägelstedt catchment.

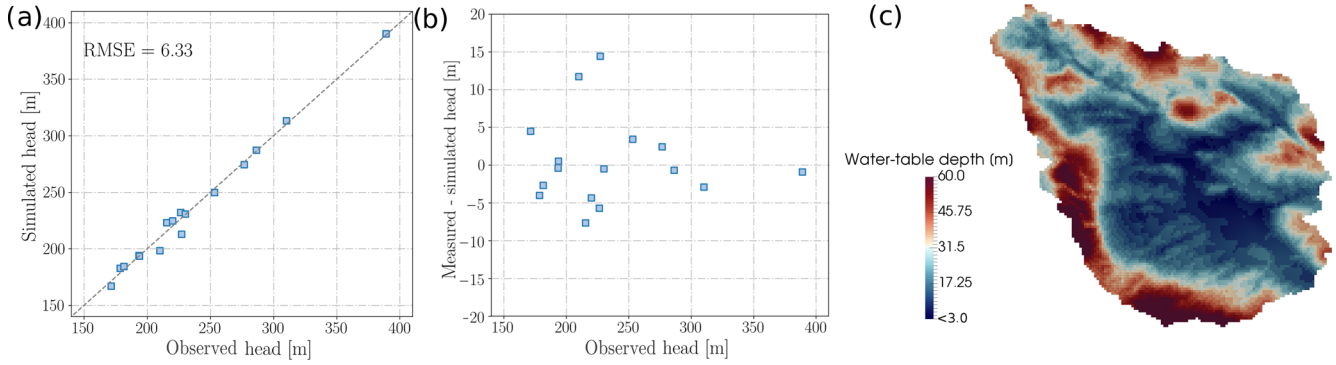

Figure 7. Illustration of steady-state groundwater model calibration and simulated heads. **(a)** Observed and simulated groundwater head (including RMSE); **(b)** difference between simulated and observed head related to the observed head values; **(c)** simulated long-term mean water table depth across the Nägelstedt catchment.

Table 1. Main hydraulic properties used in the case study under the default mHM-generated recharge scenario.

Geological units	Hydraulic conductivity ($m\,s^{-1}$)			Specific yield (–)	Specific storage (m^{-1})
	Lower limit	Upper limit	Calibrated value ($m\,s^{-1}$)		
Km	1.0×10^{-6}	5.5×10^{-3}	1.844×10^{-5}	–	1×10^{-6}
Ku	1.0×10^{-7}	3.4×10^{-4}	2.848×10^{-5}	–	1×10^{-6}
Mo1	8.0×10^{-8}	2.0×10^{-3}	3.570×10^{-5}	0.10	1×10^{-6}
Mm1	1.0×10^{-7}	9.0×10^{-4}	3.594×10^{-5}	–	1×10^{-6}
Mu1	5.0×10^{-9}	2.0×10^{-4}	6.202×10^{-6}	–	1×10^{-6}
Mo2	1.0×10^{-8}	5.0×10^{-4}	3.570×10^{-6}	–	1×10^{-6}
Mm2	3.0×10^{-8}	9.0×10^{-5}	3.594×10^{-6}	–	1×10^{-6}
Mu2	5.0×10^{-10}	2.0×10^{-5}	6.202×10^{-7}	–	1×10^{-6}
Soil	5.0×10^{-5}	1.0×10^{-2}	6.617×10^{-5}	0.10	–
Alluvium	4.0×10^{-5}	1.0×10^{-2}	3.219×10^{-4}	0.18	–

recharge simulated by mHM agrees quite well with estimates from the Hydrological Atlas of Germany (Zink et al., 2017).

Figure 9a shows the distribution of monthly groundwater recharge and monthly baseflow. Over the entire year, groundwater inflow (recharge) and outflow (baseflow) are balanced, exhibiting a mean value of 8 mm $month^{-1}$. The difference between the two values is merely 2 %. Figure 9a, however, indicates that the distribution of monthly groundwater recharge is skewed to the right, whereas the distribution of monthly baseflow is more peaked. Figure 9b depicts the time series of groundwater recharge and baseflow, which further demonstrates that the deviation of monthly groundwater recharge is larger than the baseflow. This phenomenon further reveals the significant buffering effect of the linear groundwater storage in mHM.

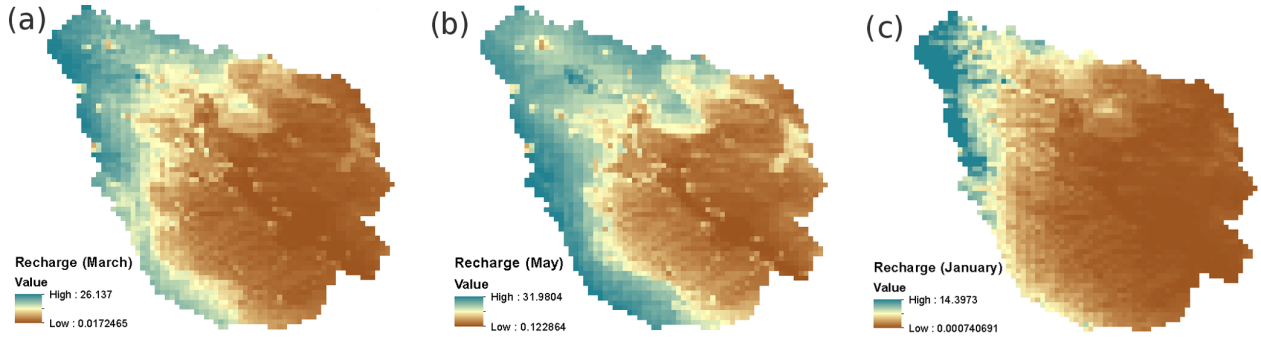

Figure 8. Spatial distributions of groundwater recharge in the Nägelstedt catchment (unit: mm month^{-1}) **(a)** in March, **(b)** in May, and **(c)** in January 2005.

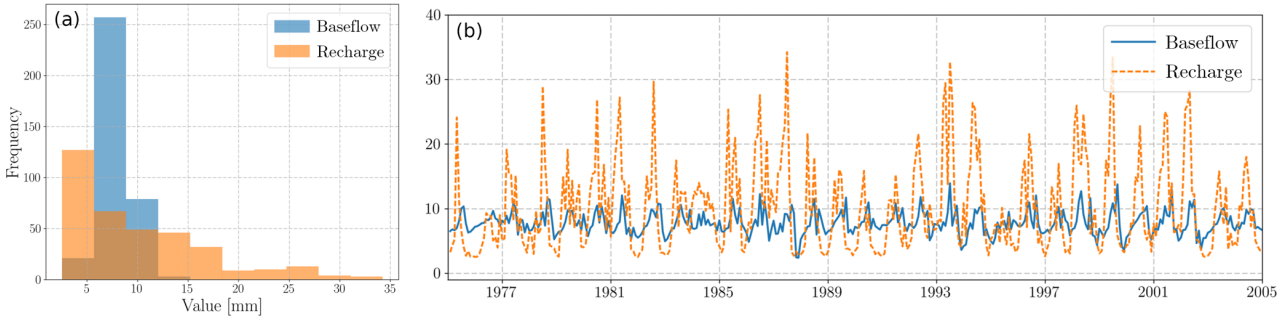

Figure 9. Analysis of groundwater inflow (recharge) and outflow (baseflow) over the Nägelstedt catchment. **(a)** Distribution of groundwater balance components. **(b)** Monthly time series of groundwater recharge and baseflow.

4.3 Model evaluation against dynamic groundwater heads

In this subsection, the head observations of several monitoring wells in the catchment were used to evaluate the model performance. We analyzed discrepancies between the modeled and observed groundwater heads by subtracting long-term mean values, $\overline{h}_{\mathrm{mod}}$ and $\overline{h}_{\mathrm{obs}}$. Four model-skill scores including the mean value, the median value, the Pearson correlation coefficient R_{cor}, and the QRE are used to evaluate the model performance.

Six wells with different geological and morphological properties were chosen as samples to exhibit the model performance (Fig. 10). Specifically, well W10 is located in the northern uplands and is near the main stream, whereas well W1 is located in the southwestern lowlands. As can be observed from Fig. 10, they provide good fits between simulated and observed heads, with a R_{cor} of 0.87 and 0.76, and a QRE of −23.34 and −1.65 %. Well W17 is located in the Lower Keuper unit, while well W16 is located in the Upper Muschelkalk formation. In these two monitoring wells, the simulations are highly correlated with observations with high values of R_{cor} (0.71 and 0.82), in spite of their different geological properties (Fig. 10). The simulation results at monitoring wells W13 (located in the northern mountainous area) and W7 (located at the northern upland) also exhibit good correspondence with the observations (Fig. 10). In general, the model is capable of capturing the historical trends of groundwater dynamics, even though the mean values of simulations and observations may deviate to some extent. Due to the limited spatial resolution and complex hydrogeological structure, this degree of discrepancy is acceptable.

4.4 Model sensitivity to different recharge scenarios

As described in Sect. 3.6, a reference recharge scenario (RR), i.e., a spatially uniform recharge scenario, is set up to assess the effect of spatial patterns of recharge on groundwater heads. In RR the steady-state groundwater model was recalibrated using the long-term mean of spatially uniform recharge (Table 2). For the purpose of showing discrepancies between two recharge scenarios, we compared the values of MAE and |QRE| at each monitoring well among the spatially distributed recharge, mR, and the RR (Fig. 11). The mean value and the median value of |QRE| were also calculated and are shown in Fig. 11. Figure 11a indicates that the MAE using the spatially distributed recharge mR (4.04 m) is lower than that using the RR (4.61 m). Considering that the only difference between the two recharge scenarios is their spatial patterns, we conclude that accounting for spatially distributed recharge provides a moderate improvement in the model.

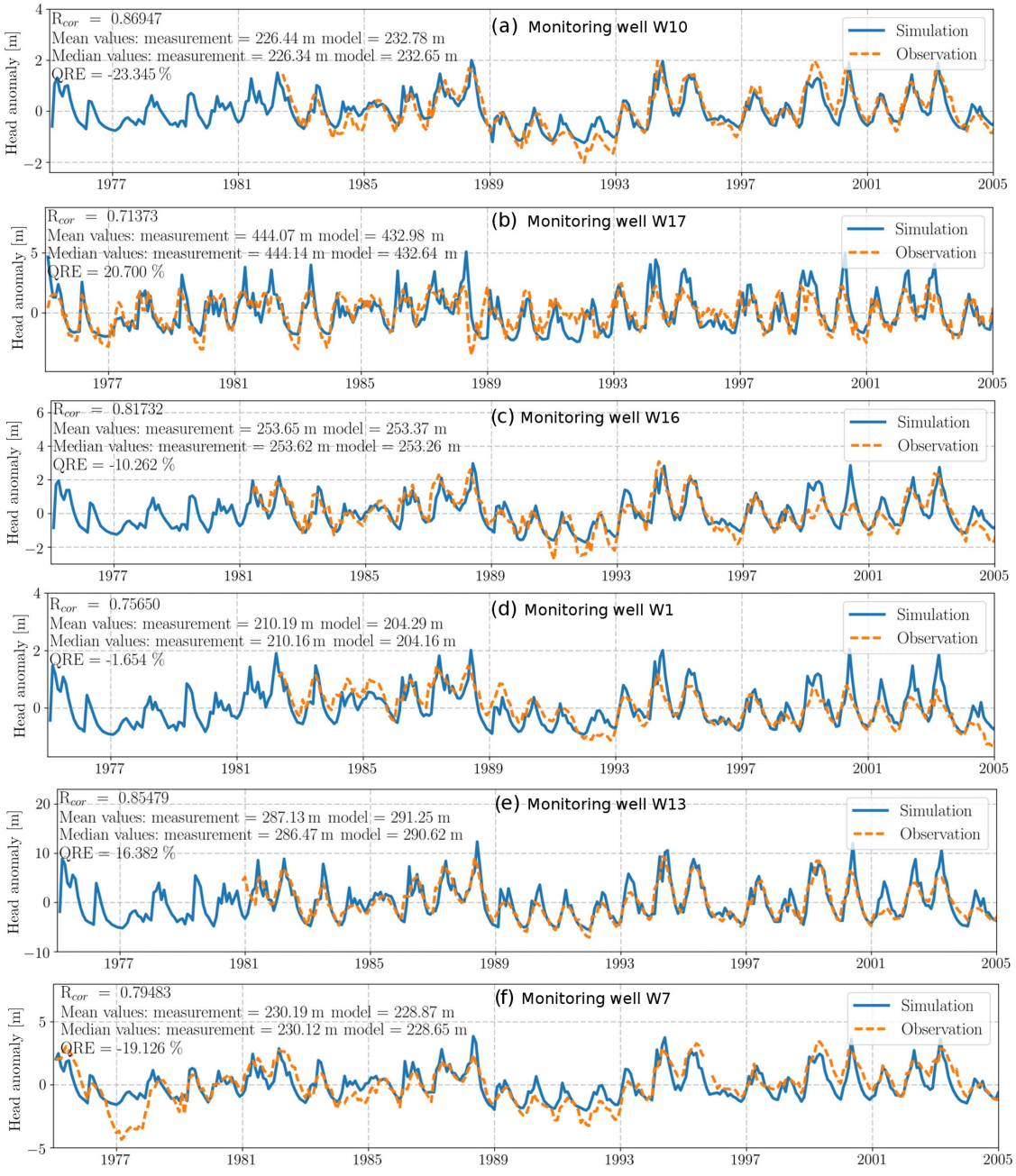

Figure 10. Comparison between measured (green dashed line) and simulated groundwater head anomalies (blue solid line). **(a)** W10 is located in the uplands, near a stream. **(b)** W17 is located in a mountainous area. **(c)** W16 is located at a hillslope in the northern uplands. **(d)** W1 is located in the lowlands. **(e)** W13 is located in the northern mountains. **(f)** W7 is located in the northern uplands.

Table 2. Hydraulic properties used in the uniform recharge scenario (RR).

Geological units	km	ku	mo1	mm1	mu1	mo2	mm2	mu2	soil	alluvium
Hydraulic conductivity ($m\,s^{-1}$)	5.023 $\times10^{-5}$	6.216 $\times10^{-5}$	8.608 $\times10^{-5}$	2.990 $\times10^{-5}$	5.316 $\times10^{-6}$	8.604 $\times10^{-6}$	2.997 $\times10^{-6}$	5.317 $\times10^{-7}$	5.239 $\times10^{-5}$	7.302 $\times10^{-4}$

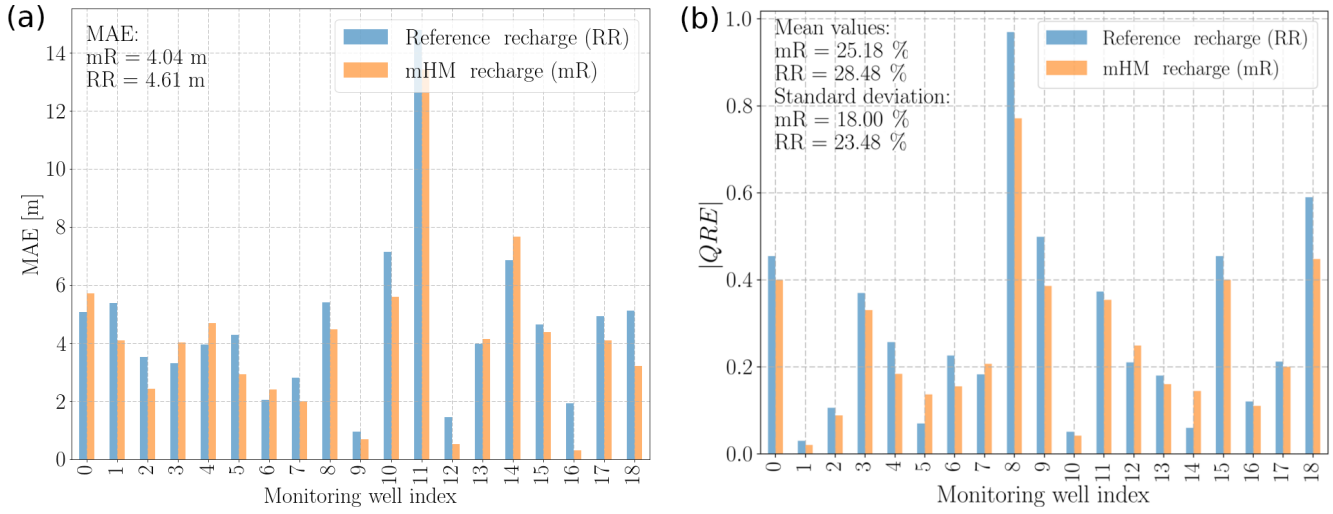

Figure 11. Bar plots of **(a)** the mean absolute error MAE and **(b)** the absolute interquartile range error |QRE| in all monitoring wells in two recharge scenarios.

Figure 11b shows the absolute values of the QRE (|QRE|) in simulations using the two recharge scenarios (mR and RR). We found that the deviation of |QRE| is significantly larger than R_{cor}, i.e., the |QRE| in two wells is abnormally higher than the other wells. The higher values of |QRE| at W8 and W18 may be caused by their proximity to model boundaries, as the two wells are located either near a river or near the catchment perimeter. This deviation indicates that accurate quantification of the amplitude of head fluctuations at certain locations is difficult, which may be due to the proximity of boundaries or complex local topography and geology. Nevertheless, 16 out of 19 wells exhibit low QREs, with the values of |QRE| in a range of ± 40 % in the spatially distributed mR scenario. We also observe a smaller mean and standard deviation of |QRE| in the spatially distributed mR than in the RR. The 19 chosen monitoring wells cover the geological units of the alluvium, Keuper, and Muschelkalk and range from high mountains to lowlands across the catchment. These results demonstrate the promising modeling capability of the model and highlight the moderately better historical matching when using a spatially distributed pattern of groundwater recharge.

Figure 12 illustrates the seasonality of groundwater heads by showing the spatial distribution of groundwater heads averaged over the spring, summer, autumn, and winter seasons. A strong spatial variability can be observed. For example, the fluctuation amplitudes of groundwater heads in the northern, eastern, and southeastern mountainous areas are larger than in the central plains area. In order to illustrate predicted groundwater levels and droughts caused by extreme climate events, we selected a meteorologically wet month (August 2002) and a meteorologically dry month (August 2003), and show the corresponding variations in groundwater heads in Fig. 12e and f. In general, the groundwater heads in the wet season are higher than the long-term mean values (Fig. 12e). The variation in groundwater heads in the dry season, however, shows a strong spatial variability. Such a strong spatial variability in groundwater head variation has also been reported by Kumar et al. (2016).

5 Discussion and conclusions

Our simulation results demonstrate that the coupled model mHM–OGS v1.0 can generally reproduce groundwater head dynamics very well. It is also able to reasonably reproduce fluctuation amplitudes of groundwater heads, although with less accuracy. The simulation results also reveal that the stochastically and physically based representations of groundwater dynamics can be intrinsically linked on the condition that the geometry and geological structure of groundwater aquifer are reasonably characterized. Compared to the good predictive capability of capturing the general trend behavior, the amplitude of head time series is hard to reproduce. This might be because local geological formations in the vicinity of monitoring wells may significantly alter local groundwater flow behavior, and thus further affect groundwater head fluctuations.

The results of this study demonstrate the successful application of the well-established hydrologic model, mHM, in estimating spatially heterogeneous groundwater recharge and baseflow at a regional scale. At a spatial scale of 10^3 km^2 (the scale in this study), the distributed recharge estimated by mHM is superior to using homogeneous recharge. mHM has been successfully applied at the continental scale covering all of Europe (Thober et al., 2015; Kumar et al., 2013b; Rakovec et al., 2016b; Zink et al., 2017). The successful application of the coupled model in this study suggests a huge potential for

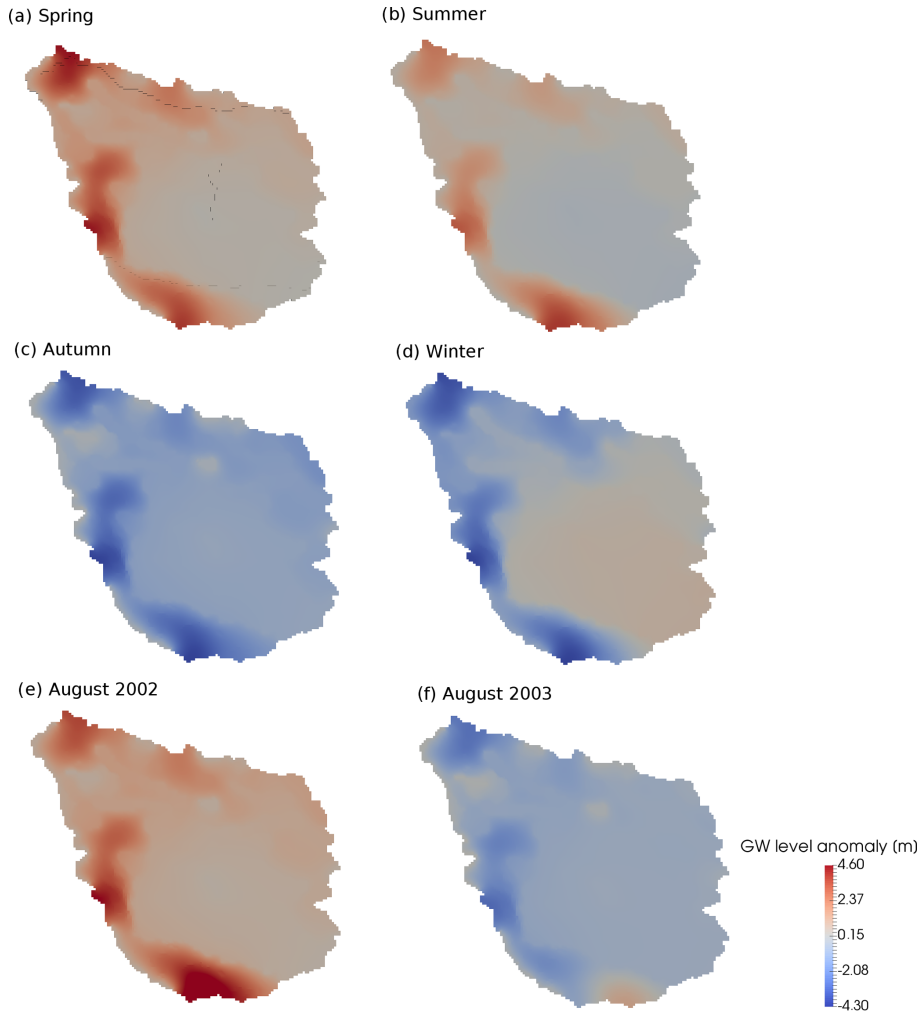

Figure 12. Seasonal variation in spatially distributed groundwater heads by their anomalies after removing the long-term mean groundwater heads (unit: m). **(a)** Long-term mean groundwater head distribution in spring; **(b)** long-term mean groundwater head distribution in summer; **(c)** long-term mean groundwater head distribution in autumn; **(d)** long-term mean groundwater head distribution in winter; **(e)** monthly mean groundwater head distribution in the wet season (August 2002); **(f)** monthly mean groundwater head distribution in the dry season (August 2003).

extending the applicability of mHM–OGS v1.0 to a larger scale (e.g., 10^4–10^6 km^2) or even a global scale.

The results of this study demonstrate a viable strategy for improving classic meso- to large-scale distributed hydrologic models, such as the current version of mHM (Samaniego et al., 2010; Kumar et al., 2013b), VIC (Liang et al., 1994), PCR-GLOBWB (Van Beek and Bierkens, 2009), and WASMOD-M (Widén-Nilsson et al., 2007). These distributed hydrologic models do not calculate spatiotemporal groundwater heads and are therefore unable to represent groundwater head dynamics in their groundwater compartment. The physical representation of groundwater flow is, however, relevant in future regional-scale and possibly global hydrologic models to accurately determine travel times, solute export from catchments, and water quality in rivers (Botter et al., 2010; Benettin et al., 2015; Van Meter et al., 2017). The coupled model mHM–OGS v1.0 also offers the potential for predicting groundwater drought in analyzing the dynamic behavior of groundwater heads. Thus, it could be a useful tool for understanding groundwater anomalies under extreme climate conditions (Kumar et al., 2016; Marx et al., 2017).

For example, building on previous work of Heße et al. (2017), who calculated travel time distributions (TTDs) using mHM, we can now expand the range of their work to the complete critical zone, which is important for comprehensively understanding particle (e.g., pollutant) transport behavior and the historical legacy in soil zone and groundwater storage (Basu et al., 2010; Beniston et al., 2014). mHM–OGS v1.0 fits well with the long-term simulation of nitrogen transport in the terrestrial water cycle. The coupled model is also able to evaluate surface water and groundwater stor-

age changes under different meteorological forcing conditions, which allows the comprehensive evaluation of hydrologic response to climate changes (e.g., global warming). Additionally, OGS demonstrates its capability in addressing thermo–hydro–mechanical–chemical (THMC) coupling processes in large-scale hydrologic cycles (not reflected in this study), which is significant for a wide range of real-world applications, including nutrient circulation, saltwater intrusion, drought, and heavy metal transport (Kalbacher et al., 2012; Selle et al., 2013; Walther et al., 2014, 2017).

In addition to improving the predictive capabilities of mHM, we can also demonstrate some improvements for the groundwater model OGS. Our results showed a modest improvement using mHM-generated recharge compared to a simpler, uniform recharge rate. We currently gain a strong advantage for the description of the top boundary condition, i.e., the recharge, which is temporal and spatially variable through the input of mHM. Even more, the recharge fluxes provided are based on mHM's phenomenological process description, which significantly better describes the surface level recharge fluxes than common approaches through recharge rates derived by empirical relations.

In this study, we have focused our efforts on extending the applicability of mHM from surface hydrology to subsurface hydrology by a simple one-way coupling. Consequently, we do not account for any feedback between river and groundwater head fluctuations. This approach is parsimonious and numerically efficient, and meanwhile fully preserves the well-tested parameterization algorithm in mHM. Unlike two-way coupling, the one-way coupling described here allows the user to expand the abilities of mHM without sacrificing any of its well-known and well-established properties. Nevertheless, in a next step, we will devote to incorporate a full, two-way coupling using the next version of the mHM–OGS model. The main limitation of one-way coupling is that the effects of a shallow depth to groundwater on actual ET, maintained by lateral groundwater flow, cannot be explicitly addressed. However, the dynamic interactions between overland flow and groundwater flow, as well as between soil moisture dynamics and groundwater dynamics, can explicitly be modeled and investigated using a full coupling scheme. This approach is open to a broader spectrum of calibration options, such as calibration by remotely sensed soil moisture data.

In conclusion, we can state that the coupled model mHM–OGS v1.0 retains the predictive capability of mHM for discharge volumes. In addition, it is capable of reproducing groundwater head dynamics. The simulation results indicate a promising predictive ability, confirmed by calibration and comparison to observed discharge and groundwater heads. Based on the historical match of discharge and groundwater heads in the case study, we conclude that the coupled model mHM–OGS v1.0 is a valuable tool for addressing many challenging problems in the field of water management, including pollutant transport and legacy, climate change, and groundwater drought.

Code availability. The coupled model mHM–OGS v1.0 can be freely acquired via the following link: https://doi.org/10.5281/zenodo.1248005. The modified source code of OpenGeoSys v5.7 can be also acquired via the above link. The mesoscale Hydrologic Model mHM (current release: 5.7) is an open-source community software and can be accessed from several mirrored repositories: SVN: http://www.ufz.de/index.php?en=40114; GitLab: https://git.ufz.de/mhm; GitHub: https://github.com/mhm-ufz.

Competing interests. The authors declare that they have no conflict of interest.

Acknowledgements. This research received funding from the Deutsche Forschungsgemeinschaft via Sonderforschungsbereich CRC 1076 AquaDiva. We kindly thank Sabine Sattler from Thuringian State office for the Environment and Geology (TLUG) for providing the geological data. We kindly thank our data providers: the German Weather Service (DWD), the Joint Research Center of the European Commission, the Federal Institute for Geosciences and Natural Resources (BGR), the European Environmental Agency (EEA), the European Water Archive (EWA), and the Global Runoff Data Centre (GRDC). We thank the two reviewers Olaf Cirpka and Edwin Sutanudjaja very much for their comprehensive reviews.

The article processing charges for this open-access publication were covered by a Research Centre of the Helmholtz Association.

Edited by: Bethanna Jackson
Reviewed by: Edwin Sutanudjaja, Olaf Arie Cirpka, and two anonymous referees

References

Ameli, A. A., Amvrosiadi, N., Grabs, T., Laudon, H., Creed, I. F., McDonnell, J. J., and Bishop, K.: Hillslope permeability architecture controls on subsurface transit time distribution and flow paths, J. Hydrol., 543, 17–30, https://doi.org/10.1016/j.jhydrol.2016.04.071, 2016.

Basu, N. B., Destouni, G., Jawitz, J. W., Thompson, S. E., Loukinova, N. V., Darracq, A., Zanardo, S., Yaeger, M., Sivapalan, M., Rinaldo, A., and Rao, P. Suresh C.: Nutrient loads exported from managed catchments reveal emergent biogeochemical stationarity, Geophys. Res. Lett., 37, L23404, doi10.1029/2010GL045168, 2010.

Benettin, P., Kirchner, J. W., Rinaldo, A., and Botter, G.: Modeling chloride transport using travel time distributions at Plynlimon, Wales, Water Resour. Res., 51, 3259–3276, https://doi.org/10.1002/2014WR016600, 2015.

Benettin, P., Soulsby, C., Birkel, C., Tetzlaff, D., Botter, G., and Rinaldo, A.: Using SAS functions and high-resolution

isotope data to unravel travel time distributions in headwater catchments, Water Resour. Res., 53, 1864–1878, https://doi.org/10.1002/2016WR020117, 2017.

Beniston, J. W., DuPont, S. T., Glover, J. D., Lal, R., and Dungait, J. A.: Soil organic carbon dynamics 75 years after land-use change in perennial grassland and annual wheat agricultural systems, Biogeochemistry, 120, 37–49, 2014.

Beyer, C., Bauer, S., and Kolditz, O.: Uncertainty assessment of contaminant plume length estimates in heterogeneous aquifers, J. Contam. Hydrol., 87, 73–95, 2006.

Bisht, G., Huang, M., Zhou, T., Chen, X., Dai, H., Hammond, G. E., Riley, W. J., Downs, J. L., Liu, Y., and Zachara, J. M.: Coupling a three-dimensional subsurface flow and transport model with a land surface model to simulate stream–aquifer–land interactions (CP v1.0), Geosci. Model Dev., 10, 4539–4562, https://doi.org/10.5194/gmd-10-4539-2017, 2017.

Botter, G., Bertuzzo, E., and Rinaldo, A.: Transport in the hydrologic response: Travel time distributions, soil moisture dynamics, and the old water paradox, Water Resour. Res., 46, 1–18, https://doi.org/10.1029/2009WR008371, 2010.

Camporese, M., Paniconi, C., Putti, M., and Orlandini, S.: Surface-subsurface flow modeling with path-based runoff routing, boundary condition-based coupling, and assimilation of multisource observation data, Water Resour. Res., 46, W02512, https://doi.org/10.1029/2008WR007536, 2010.

Cirpka, O. A. and Attinger, S.: Effective dispersion in heterogeneous media under random transient flow conditions, Water Resour. Res., 39, 1257, https://doi.org/10.1029/2002WR001931, 2003.

Dagan, G.: Flow and transport in porous formations, Springer Science & Business Media, 2012.

Danesh-Yazdi, M., Klaus, J., Condon, L. E., and Maxwell, R. M.: Bridging the gap between numerical solutions of travel time distributions and analytical storage selection functions, Hydrol. Proc., 32, 1063–1076, https://doi.org/10.1002/hyp.11481, 2018.

de Marsily, G., Delay, F., Gonçalvès, J., Renard, P., Teles, V., and Violette, S.: Dealing with spatial heterogeneity, Hydrogeol. J., 13, 161–183, https://doi.org/10.1007/s10040-004-0432-3, 2005.

Delfs, J. O., Blumensaat, F., Wang, W., Krebs, P., and Kolditz, O.: Coupling hydrogeological with surface runoff model in a Poltva case study in Western Ukraine, Environ. Earth Sci., 65, 1439–1457, https://doi.org/10.1007/s12665-011-1285-4, 2012.

Doherty, J.: PEST: a unique computer program for model-independent parameter optimisation, Water Down Under 94: Groundwater/Surface Hydrology Common Interest Papers, Preprints of Papers, p. 551, 1994.

Engdahl, N. B. and Maxwell, R. M.: Quantifying changes in age distributions and the hydrologic balance of a high-mountain watershed from climate induced variations in recharge, J. Hydrol., 522, 152–162, https://doi.org/10.1016/j.jhydrol.2014.12.032, 2015.

Ferguson, I. M., Jefferson, J. L., Maxwell, R. M., and Kollet, S. J.: Effects of root water uptake formulation on simulated water and energy budgets at local and basin scales, Environ. Earth Sci., 75, 1–15, 2016.

Fischer, T., Naumov, D., Sattler, S., Kolditz, O., and Walther, M.: GO2OGS 1.0: a versatile workflow to integrate complex geological information with fault data into numerical simulation models, Geosci. Model Dev., 8, 3681–3694, https://doi.org/10.5194/gmd-8-3681-2015, 2015.

Gräbe, A., Rödiger, T., Rink, K., Fischer, T., Sun, F., Wang, W., Siebert, C., and Kolditz, O.: Numerical analysis of the groundwater regime in the western Dead Sea escarpment, Israel+ West Bank, Environ. Earth Sci., 69, 571–585, 2013.

Green, T. R., Taniguchi, M., Kooi, H., Gurdak, J. J., Allen, D. M., Hiscock, K. M., Treidel, H., and Aureli, A.: Beneath the surface of global change: Impacts of climate change on groundwater, J. Hydrol., 405, 532–560, 2011.

Gulden, L. E., Rosero, E., Yang, Z. L., Rodell, M., Jackson, C. S., Niu, G. Y., Yeh, P. J. F., and Famiglietti, J.: Improving land-surface model hydrology: Is an explicit aquifer model better than a deeper soil profile?, Geophys. Res. Lett., 34, 1–5, https://doi.org/10.1029/2007GL029804, 2007.

Hale, V. C. and McDonnell, J. J.: Effect of bedrock permeability on stream base flow mean transit time scaling relations: 1. A multiscale catchment intercomparison, Water Resour. Res., 52, 1358–1374, 2016.

Hargreaves, G. H. and Samani, Z. A.: Reference crop evapotranspiration from temperature, Appl. Eng. Agric., 1, 96–99, 1985.

He, W., Beyer, C., Fleckenstein, J. H., Jang, E., Kolditz, O., Naumov, D., and Kalbacher, T.: A parallelization scheme to simulate reactive transport in the subsurface environment with OGS#IPhreeqc 5.5.7-3.1.2, Geosci. Model Dev., 8, 3333–3348, https://doi.org/10.5194/gmd-8-3333-2015, 2015.

Heße, F., Zink, M., Kumar, R., Samaniego, L., and Attinger, S.: Spatially distributed characterization of soil-moisture dynamics using travel-time distributions, Hydrol. Earth Syst. Sci., 21, 549–570, https://doi.org/10.5194/hess-21-549-2017, 2017.

Hrachowitz, M. and Clark, M. P.: HESS Opinions: The complementary merits of competing modelling philosophies in hydrology, Hydrol. Earth Syst. Sci., 21, 3953–3973, https://doi.org/10.5194/hess-21-3953-2017, 2017.

Huang, S., Kumar, R., Flörke, M., Yang, T., Hundecha, Y., Kraft, P., Gao, C., Gelfan, A., Liersch, S., Lobanova, A., Strauch, M., van Ogtrop, F., Reinhardt, J., Haberlandt, U., and Krysanova, V.: Evaluation of an ensemble of regional hydrological models in 12 large-scale river basins worldwide, Clim. Change, 141, 381–397, https://doi.org/10.1007/s10584-016-1841-8, 2017.

Hunt, R. J., Walker, J. F., Selbig, W. R., Westenbroek, S. M., and Regan, R. S.: Simulation of Climate – Change effects on streamflow, Lake water budgets, and stream temperature using GSFLOW and SNTEMP, Trout Lake Watershed, Wisconsin, USGS Scientific Investigations Report, 2013–5159, 2013.

Hwang, H. T., Park, Y. J., Sudicky, E. A., and Forsyth, P. A.: A parallel computational framework to solve flow and transport in integrated surface-subsurface hydrologic systems, Environ. Model. Softw., 61, 39–58, https://doi.org/10.1016/j.envsoft.2014.06.024, 2014.

Ivano, V. Y., Vivoni, E. R., Bras, R. L., and Entekhabi, D.: Catchment hydrologic response with a fully distributed triangulated irregular network model, Water Resour. Res., 40, W11102, https://doi.org/10.1029/2004WR003218, 2004.

Kalbacher, T., Delfs, J. O., Shao, H., Wang, W., Walther, M., Samaniego, L., Schneider, C., Kumar, R., Musolff, A., Centler, F., Sun, F., Hildebrandt, A., Liedl, R., Borchardt, D., Krebs, P., and Kolditz, O.: The IWAS-ToolBox: Software coupling for an integrated water resources management, Environ. Earth Sci., 65, 1367–1380, https://doi.org/10.1007/s12665-011-1270-y, 2012.

Kohlhepp, B., Lehmann, R., Seeber, P., Küsel, K., Trumbore, S. E., and Totsche, K. U.: Aquifer configuration and geostructural links control the groundwater quality in thin-bedded carbonate-siliciclastic alternations of the Hainich CZE, central Germany, Hydrol. Earth Syst. Sci., 21, 6091–6116, https://doi.org/10.5194/hess-21-6091-2017, 2017.

Kolditz, O., Bauer, S., Bilke, L., Böttcher, N., Delfs, J. O., Fischer, T., Görke, U. J., Kalbacher, T., Kosakowski, G., McDermott, C. I., Park, C. H., Radu, F., Rink, K., Shao, H., Shao, H. B., Sun, F., Sun, Y. Y., Singh, A. K., Taron, J., Walther, M., Wang, W., Watanabe, N., Wu, Y., Xie, M., Xu, W., and Zehner, B.: OpenGeoSys: an open-source initiative for numerical simulation of thermo-hydro-mechanical/chemical (THM/C) processes in porous media, Enviro. Earth Sci., 67, 589–599, https://doi.org/10.1007/s12665-012-1546-x, 2012.

Kolditz, O., Shao, H., Wang, W., and Bauer, S.: Thermo-hydro-mechanical-chemical processes in fractured porous media: modelling and benchmarking, Springer, 2016.

Koren, V., Reed, S., Smith, M., Zhang, Z., and Seo, D.-J.: Hydrology laboratory research modeling system (HL-RMS) of the US national weather service, J. Hydrol., 291, 297–318, 2004.

Kumar, M., Duffy, C. J., and Salvage, K. M.: A Second-Order Accurate, Finite Volume-Based, Integrated Hydrologic Modeling (FIHM) Framework for Simulation of Surface and Subsurface Flow, Vadose Zone J., 8, 873, https://doi.org/10.2136/vzj2009.0014, 2009.

Kumar, R., Livneh, B., and Samaniego, L.: Toward computationally efficient large-scale hydrologic predictions with a multiscale regionalization scheme, Water Resour. Res., 49, 5700–5714, https://doi.org/10.1002/wrcr.20431, 2013a.

Kumar, R., Samaniego, L., and Attinger, S.: Implications of distributed hydrologic model parameterization on water fluxes at multiple scales and locations, Water Resour. Res., 49, 360–379, 2013b.

Kumar, R., Musuuza, J. L., Van Loon, A. F., Teuling, A. J., Barthel, R., Ten Broek, J., Mai, J., Samaniego, L., and Attinger, S.: Multiscale evaluation of the Standardized Precipitation Index as a groundwater drought indicator, Hydrol. Earth Syst. Sci., 20, 1117–1131, https://doi.org/10.5194/hess-20-1117-2016, 2016.

Kurtz, W., He, G., Kollet, S. J., Maxwell, R. M., Vereecken, H., and Hendricks Franssen, H.-J.: TerrSysMP-PDAF (version 1.0): a modular high-performance data assimilation framework for an integrated land surface-subsurface model, Geosci. Model Dev., 9, 1341–1360, https://doi.org/10.5194/gmd-9-1341-2016, 2016.

Küsel, K., Totsche, K. U., Trumbore, S. E., Lehmann, R., Steinhäuser, C., and Herrmann, M.: How deep can surface signals be traced in the critical zone? Merging biodiversity with biogeochemistry research in a central German Muschelkalk landscape, Front. Earth Sci., 4, 32, https://doi.org/10.3389/feart.2016.00032, 2016.

Liang, X., Lettenmaier, D. P., Wood, E. F., and Burges, S. J.: A simple hydrologically based model of land surface water and energy fluxes for general circulation models, J. Geophys. Res.-Atmos., 99, 14415–14428, 1994.

Lindström, G., Johansson, B., Persson, M., Gardelin, M., and Bergström, S.: Development and test of the distributed HBV-96 hydrological model, J. Hydrol., 201, 272–288, 1997.

Markstrom, S. L., Niswonger, R. G., Regan, R. S., Prudic, D. E., and Barlow, P. M.: GSFLOW-Coupled Ground-Water and Surface-Water Flow Model Based on the Integration of the Precipitation-Runoff Modeling System (PRMS) and the Modular Ground-Water Flow Model (MODFLOW-2005), US Geological Survey, 240 pp., available at: http://pubs.er.usgs.gov/publication/tm6D1 (last access: 30 May 2018), 2008.

Marx, A., Kumar, R., Thober, S., Rakovec, O., Wanders, N., Zink, M., Wood, E. F., Pan, M., Sheffield, J., and Samaniego, L.: Climate change alters low flows in Europe under global warming of 1.5, 2, and 3 °C, Hydrol. Earth Syst. Sci., 22, 1017–1032, https://doi.org/10.5194/hess-22-1017-2018, 2018.

Maxwell, R. M. and Miller, N. L.: Development of a coupled land surface and groundwater model, J. Hydrometeorol., 6, 233–247, https://doi.org/10.1175/JHM422.1, 2005.

Maxwell, R. M., Condon, L. E., and Kollet, S. J.: A high-resolution simulation of groundwater and surface water over most of the continental US with the integrated hydrologic model ParFlow v3, Geosci. Model Dev., 8, 923–937, https://doi.org/10.5194/gmd-8-923-2015, 2015.

McLachlan, P., Chambers, J., Uhlemann, S., and Binley, A.: Geophysical characterisation of the groundwater–surface water interface, Adv. Water Resour., 109, 302–319, https://doi.org/10.1016/j.advwatres.2017.09.016, 2017.

Niu, G.-Y., Yang, Z.-L., Mitchell, K. E., Chen, F., Ek, M. B., Barlage, M., Kumar, A., Manning, K., Niyogi, D., Rosero, E., Tewari, M., and Xia, Y.: The community Noah land surface model with multiparameterization options (Noah-MP): 1. Model description and evaluation with local-scale measurements, J. Geophys. Res.-Atmos., 116, D12109, https://doi.org/10.1029/2010JD015139, 2011.

Panday, S. and Huyakorn, P. S.: A fully coupled physically-based spatially-distributed model for evaluating surface/subsurface flow, Adv. Water Resour., 27, 361–382, https://doi.org/10.1016/j.advwatres.2004.02.016, 2004.

Paniconi, C. and Putti, M.: Physically based modeling in catchment hydrology at 50: Survey and outlook, Water Resour. Res., 51, 7090–7129, https://doi.org/10.1002/2015WR017780, 2015.

Park, C. H., Beyer, C., Bauer, S., and Kolditz, O.: Using global node-based velocity in random walk particle tracking in variably saturated porous media: Application to contaminant leaching from road constructions, Environ. Geol., 55, 1755–1766, https://doi.org/10.1007/s00254-007-1126-7, 2008.

Phi, S., Clarke, W., and Li, L.: Laboratory and numerical investigations of hillslope soil saturation development and runoff generation over rainfall events, J. Hydrol., 493, 1–15, https://doi.org/10.1016/j.jhydrol.2013.04.009, 2013.

Qu, Y. and Duffy, C. J.: A semidiscrete finite volume formulation for multiprocess watershed simulation, Water Resour. Res., 43, W08419, https://doi.org/10.1029/2006WR005752, 2007.

Rakovec, O., Kumar, R., Attinger, S., and Samaniego, L.: Improving the realism of hydrologic model functioning through multivariate parameter estimation, Water Resour. Res., 52, 7779–7792, 2016a.

Rakovec, O., Kumar, R., Mai, J., Cuntz, M., Thober, S., Zink, M., Attinger, S., Schäfer, D., Schrön, M., and Samaniego, L.: Multiscale and multivariate evaluation of water fluxes and states over European river basins, J. Hydrometeorol., 17, 287–307, 2016b.

Refsgaard, J. C. and Storm, B.: Mike SHE, Computer models of watershed hydrology, 1, 809–846, 1995.

Rigon, R., Bertoldi, G., and Over, T. M.: GEOtop: A Distributed Hydrological Model with Coupled Water and Energy Budgets, J. Hydrometeorol., 7, 371–388, https://doi.org/10.1175/JHM497.1, 2006.

Samaniego, L., Kumar, R., and Attinger, S.: Multiscale parameter regionalization of a grid-based hydrologic model at the mesoscale, Water Resour. Res., 46, W05523, https://doi.org/10.1029/2008WR007327, 2010.

Samaniego, L., Kumar, R., Thober, S., Rakovec, O., Zink, M., Wanders, N., Eisner, S., Müller Schmied, H., Sutanudjaja, E. H., Warrach-Sagi, K., and Attinger, S.: Toward seamless hydrologic predictions across spatial scales, Hydrol. Earth Syst. Sci., 21, 4323–4346, https://doi.org/10.5194/hess-21-4323-2017, 2017.

Scibek, J. and Allen, D.: Modeled impacts of predicted climate change on recharge and groundwater levels, Water Resour. Res., 42, W11405, https://doi.org/10.1029/2005WR004742, 2006.

Seidel, G.: Geologie von Thüringen, Erdkunde, 58 pp., 2004.

Selle, B., Rink, K., and Kolditz, O.: Recharge and discharge controls on groundwater travel times and flow paths to production wells for the Ammer catchment in southwestern Germany, Environ. Earth Sci., 69, 443–452, https://doi.org/10.1007/s12665-013-2333-z, 2013.

Shao, H., Dmytrieva, S. V., Kolditz, O., Kulik, D. A., Pfingsten, W., and Kosakowski, G.: Modeling reactive transport in non-ideal aqueous-solid solution system, Appl. Geochem., 24, 1287–1300, https://doi.org/10.1016/j.apgeochem.2009.04.001, 2009.

Shao, H., Nagel, T., Roßkopf, C., Linder, M., Wörner, A., and Kolditz, O.: Non-equilibrium thermo-chemical heat storage in porous media: Part 2–A 1D computational model for a calcium hydroxide reaction system, Energy, 60, 271–282, 2013.

Shen, C. and Phanikumar, M. S.: A process-based, distributed hydrologic model based on a large-scale method for surface-subsurface coupling, Adv. Water Resour., 33, 1524–1541, https://doi.org/10.1016/j.advwatres.2010.09.002, 2010.

Smerdon, B. D., Mendoza, C. A., and Devito, K. J.: Simulations of fully coupled lake-groundwater exchange in a subhumid climate with an integrated hydrologic model, Water Resour. Res., 43, W01416, https://doi.org/10.1029/2006WR005137, 2007.

Spanoudaki, K., Stamou, A. I., and Nanou-Giannarou, A.: Development and verification of a 3-D integrated surface water–groundwater model, J. Hydrol., 375, 410–427, https://doi.org/10.1016/j.jhydrol.2009.06.041, 2009.

Sun, F., Shao, H., Kalbacher, T., Wang, W., Yang, Z., Huang, Z., and Kolditz, O.: Groundwater drawdown at Nankou site of Beijing Plain: model development and calibration, Environ. Earth Sci., 64, 1323–1333, https://doi.org/10.1007/s12665-011-0957-4, 2011.

Sutanudjaja, E. H., van Beek, L. P. H., de Jong, S. M., van Geer, F. C., and Bierkens, M. F. P.: Large-scale groundwater modeling using global datasets: a test case for the Rhine-Meuse basin, Hydrol. Earth Syst. Sci., 15, 2913–2935, https://doi.org/10.5194/hess-15-2913-2011, 2011.

Sutanudjaja, E. H., Van Beek, L. P. H., De Jong, S. M., Van Geer, F. C., and Bierkens, M. F. P.: Calibrating a large-extent high-resolution coupled groundwater-land surface model using soil moisture and discharge data, Water Resour. Res., 50, 687–705, https://doi.org/10.1002/2013WR013807, 2014.

Therrien, R., McLaren, R. G., Sudicky, E. A., and Panday, S. M.: HydroGeoSphere: A three-dimensional numerical model describing fully-integrated subsurface and surface flow and solute transport, Groundwater Simulations Group, University of Waterloo, Waterloo, ON, 2010.

Thober, S., Kumar, R., Sheffield, J., Mai, J., Schäfer, D., and Samaniego, L.: Seasonal Soil Moisture Drought Prediction over Europe Using the North American Multi-Model Ensemble (NMME), J. Hydrometeorol., 16, 2329–2344, https://doi.org/10.1175/JHM-D-15-0053.1, 2015.

Van Beek, L. and Bierkens, M. F.: The global hydrological model PCR-GLOBWB: conceptualization, parameterization and verification, Utrecht University, Utrecht, the Netherlands, 2009.

Van Meter, K. J., Basu, N. B., and Van Cappellen, P.: Two centuries of nitrogen dynamics: Legacy sources and sinks in the Mississippi and Susquehanna River Basins, Global Biogeochem. Cy., 31, 2–23, https://doi.org/10.1002/2016GB005498, 2017.

VanderKwaak, J. E. and Loague, K.: Hydrologic-response simulations for the R-5 catchment with a comprehensive physics-based model, Water Resour. Res., 37, 999–1013, https://doi.org/10.1029/2000WR900272, 2001.

Walther, M., Delfs, J.-O., Grundmann, J., Kolditz, O., and Liedl, R.: Saltwater intrusion modeling: Verification and application to an agricultural coastal arid region in Oman, J. Comput. Appl. Math., 236, 4798–4809, https://doi.org/10.1016/j.cam.2012.02.008, 2012.

Walther, M., Solpuker, U., Böttcher, N., Kolditz, O., Liedl, R., and Schwartz, F. W.: Description and verification of a novel flow and transport model for silicate-gel emplacement, J. Contam. Hydrol., 157, 1–10, 2014.

Walther, M., Graf, T., Kolditz, O., Liedl, R., and Post, V.: How significant is the slope of the sea-side boundary for modelling seawater intrusion in coastal aquifers?, J. Hydrol., 551, 648–659, https://doi.org/10.1016/j.jhydrol.2017.02.031, 2017.

Wang, W., Kosakowski, G., and Kolditz, O.: A parallel finite element scheme for thermo-hydro-mechanical (THM) coupled problems in porous media, Comput. Geosci., 35, 1631–1641, https://doi.org/10.1016/j.cageo.2008.07.007, 2009.

Wang, W., Kolditz, O., and Nagel, T.: Parallel finite element modelling of multi-physical processes in thermochemical energy storage devices, Appl. Energ., 185, 1954–1964, 2017.

Wechsung, F.: Auswirkungen des globalen Wandels auf Wasser, Umwelt und Gesellschaft im Elbegebiet, vol. 6, Weißensee Verlag, 2005.

Weill, S., Mouche, E., and Patin, J.: A generalized Richards equation for surface/subsurface flow modelling, J. Hydrol., 366, 9–20, https://doi.org/10.1016/j.jhydrol.2008.12.007, 2009.

Widén-Nilsson, E., Halldin, S., and Xu, C.-y.: Global water-balance modelling with WASMOD-M: Parameter estimation and regionalisation, J. Hydrol., 340, 105–118, 2007.

Wood, E. F., Lettenmaier, D., Liang, X., Nijssen, B., and Wetzel, S. W.: Hydrological modeling of continental-scale basins, Annu. Rev. Earth Pl. Sc., 25, 279–300, 1997.

Zech, A., Zehner, B., Kolditz, O., and Attinger, S.: Impact of Heterogeneous Permeability Distribution on the Groundwater Flow Systems of a Small Sedimentary Basin, J. Hydrol., 532, 90–101, https://doi.org/10.1016/j.jhydrol.2015.11.030, 2015.

Zink, M., Kumar, R., Cuntz, M., and Samaniego, L.: A high-resolution dataset of water fluxes and states for Germany accounting for parametric uncertainty, Hydrol. Earth Syst. Sci., 21, 1769–1790, https://doi.org/10.5194/hess-21-1769-2017, 2017.